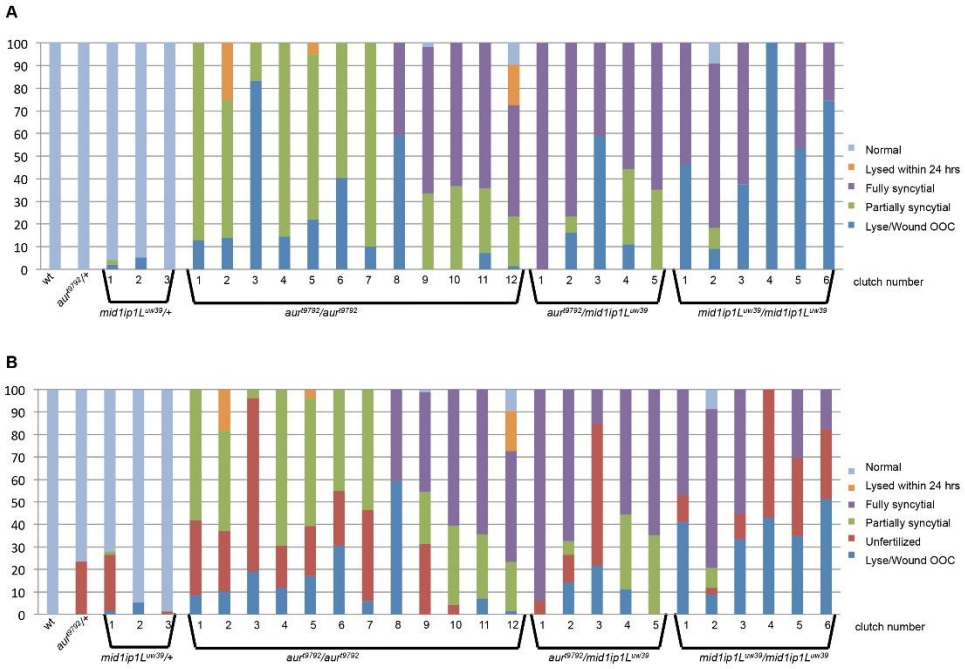

Supplementary Figure 1: Phenotypic spectrum associated with *aura*^{t9792} and *mid1ip1L*^{uw39} mutant alleles. A) Embryos from different *aur*^{t9792}/*aur*^{t9792} homozygous mothers, *aur*^{t9792}/*mid1ip1L*^{uw39} transheterozygous mothers and homozygous *mid1ip1L*^{uw39}/ *mid1ip1L*^{uw39} mothers exhibit a similar spectrum of defects. Embryos from an *aur*/+ heterozygous sibling females were indistinguishable from wild-type. Cleavage stage phenotypes are presented as the fraction of embryos that exhibit aberrant syncytial regions in the blastula-stage embryo (2.5 hpf), since the observed expanded syncytial space reflects defects in the completion of cytokinesis and associated membrane regression during blastomeric divisions (Yabe et al., 2007; Yabe et al., 2009; Nair et al., 2013). Normal, partially syncytial and fully syncytial embryos correspond to embryos with normal furrow formation, partial furrow formation and no furrow formation during the early (2- to 8-cell) cleavage stages. "Lysed within 24 hrs" embryos exhibit apparently normal morphology at 2.5 hpf but undergo lysis before 24 hpf. "Normal" embryos appear normal at 24 hpf. The fraction of apparently unfertilized embryos (exhibiting no symmetric cleavage during furrow initiation) varies even among wild-type clutches and appears unrelated to phenotypic strength in *aura* mutant clutches, and has been excluded from the presented data for clarity. The phenotypic range follows the order *mid1ip1L*^{uw39}/ *mid1ip1L*^{uw39} (strongest) > *aur*^{n9792}/ *mid1ip1L*^{uw39} > *aur*^{n9792}/*aur*^{n9792} (weakest), suggesting that that the *aur*^{n9792} allele is hypomorphic. Clutches from females heterozygous for the wild-type and either mutant allele appear normal. B) Data as in (A) but including the fraction of apparently unfertilized embryos.

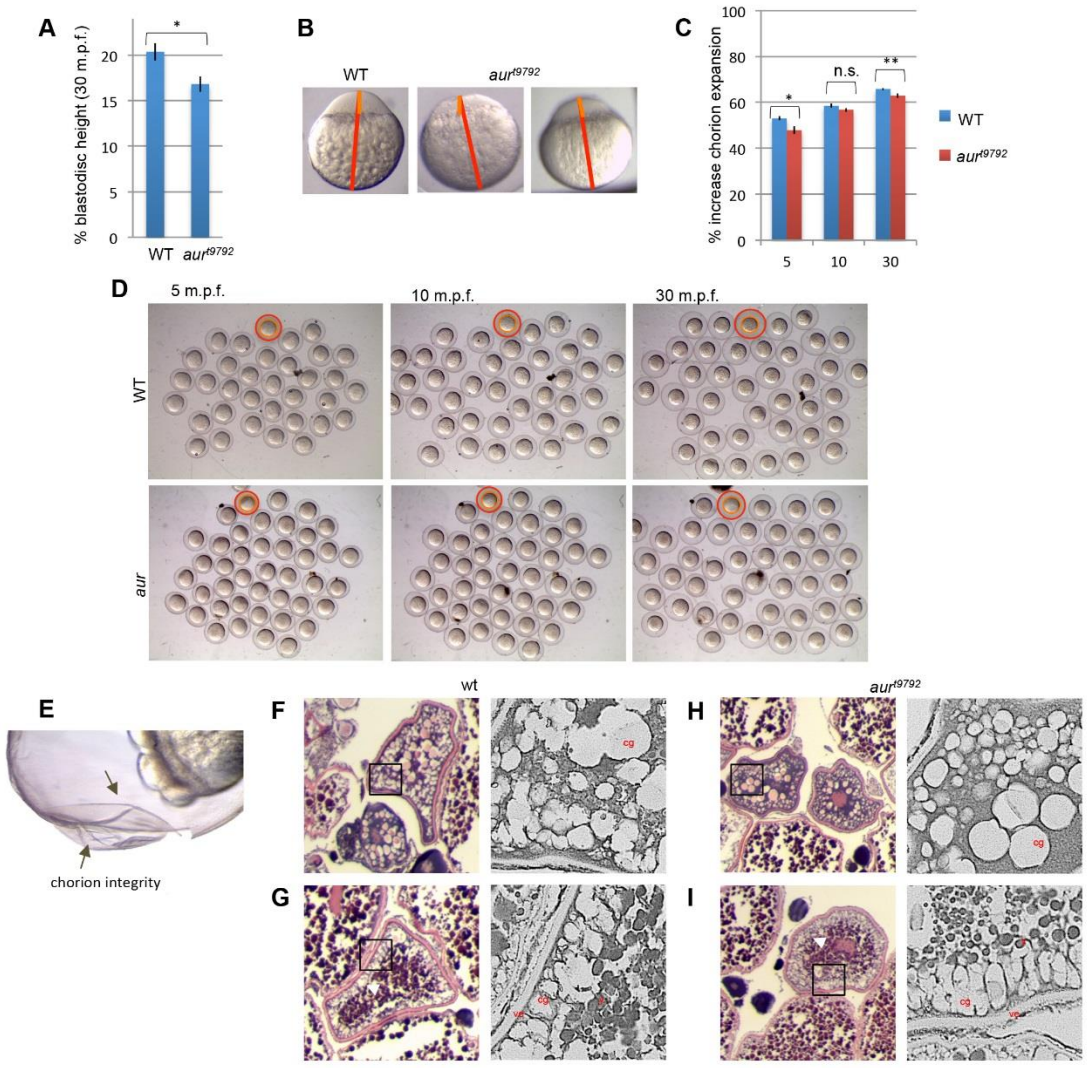

Supplementary Figure 2: Blastodisc height and chorion expansion in wild-type and *aura* mutant embryos. (A,B) Blastodisc height in wild-type (n=39) and *aura* mutant embryos (n=42) (A). Height (orange lines, B) was measured as a percentage of the whole embryo length (red lines) at 30 mpf. Average blastodisc height in mutants is mildly yet statistically significantly reduced compared to wild-type (t-test, p-value=0.020). (C,D) Average chorion expansion in mutants is mildly yet statistically significantly reduced compared to wild-type in two of three measured time points (t-test type, p- values: 5 mpf: 0.010, 10 mpf: 0.16; 30 mpf: 0.0099). (C). Chorion lifting was measured by subtracting the area of the embryo (orange circle in D) from the area of the chorion (red circle in D). A fraction of *aura* mutant embryos (60%, n=1096) exhibit chorion fragility in which it separates as sublayers (E, arrows). Although we can not rule out other interpretations, this chorion fragility phenotype that can be interpreted as a consequence of reduced chorionic protein modification of chorion

sublayers (Ulrich, 1969; Hart and Collins, 1991; Selman et al., 1993) due to decreased CG release in *aura* mutants. Embryos were a random collection from 3 females per genotype. Bars represent standard error values. Brackets reflect degree of statistical significance, with p-values < 0.01 (**), 0.01 - 0.05 (*), and > 0.05 (n.s.). Ovary sections of wild-type (pre- and post-CG (cg) accumulation at the cortex, just below the vitelline envelope (ve). F,G) and mutant (pre- and post-CG accumulation). H,I) Ovaries showing that CGs (arrowheads) are aligned at the cortex, and yolk (y) morphology is normal in *aura* oocytes.

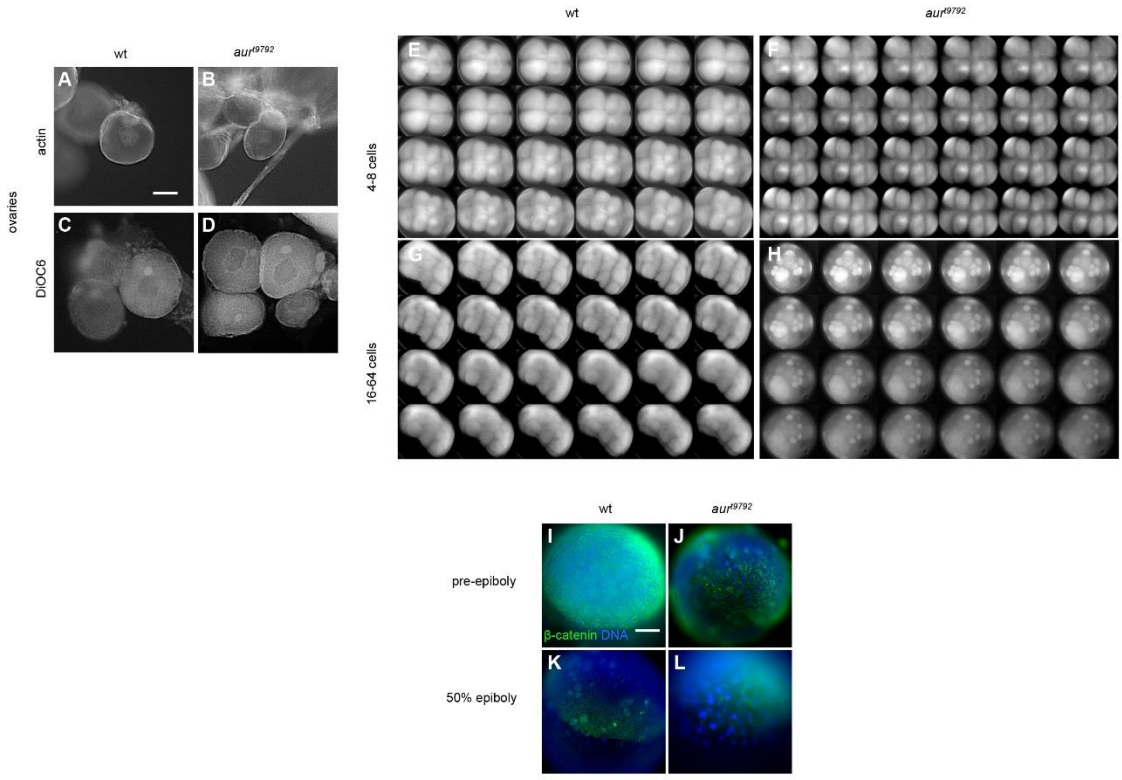

Supplementary Figure 3: Overview of landmarks of oogenesis and early cleavage in *aura* mutants. (A-D) Landmarks during oogenesis appear normal in *aura* oocytes. (A,B) Accumulation of F-actin appears unaffected normal in stage I *aura* mutant oocytes (wt= 5/5, *aura*= 4/4). Accumulation and localization of mitochondria and ER, marking the Balbiani body (Gupta et al. 2010), appears normal in stage I *aura* mutant oocytes (wt= 23/23, *aura*= 20/20). (E-H) Loss of blastomere cellular adhesion in *aura* mutant embryos. Live imaging of F-actin in embryos using the Life Act transgene in wild-type (3/3 E,G) and *aura* mutant line (3/3 F,H). The cellular pattern is relatively normal up to the 8-cell stage, as expected since cell adhesion is a property of mature furrows that become fully formed for the first cell cycle at this stage. By late 16-cell stage, *aura* embryos begin to display rounded and loose cells, which can be of varying sizes, consistent with defects in late cytokinesis involving reduced adhesive membrane deposition and membrane regression. The normal cleavage pattern up to the 8-cell stage indicates that the spindle orientation that results in the typically invariant cleavage pattern is normal. Images were taken in one minute intervals from 60 mpf to 85 mpf (E,F) and two minute intervals from 90 mpf to 120 mpf (G,H). (I-L) In *aura* mutants, DNA masses undergo epiboly-like vegetal movement in the absence of cellular layers. The DNA masses are uneven, likely due to the lack of cell membranes in these embryos and

consequent mis-segregation of chromosomes by neighboring asters. Top panels (I,J, animal view) are pre-epiboly stages (4 hpf), bottom panels (K,L, side view) are 50% epiboly stages (5.5 hpf). DNA masses in *aura* mutants (J,L) appear at vegetal levels consistent with an epibolic-like movement, similar to migration in wild-type (I,K) except with reduced cell membrane formation. ß-catenin (green, highlights membrane, which is reduced in mutants), DNA (blue). Scale bars: A-D: 25 µm; I-L: 100 µm

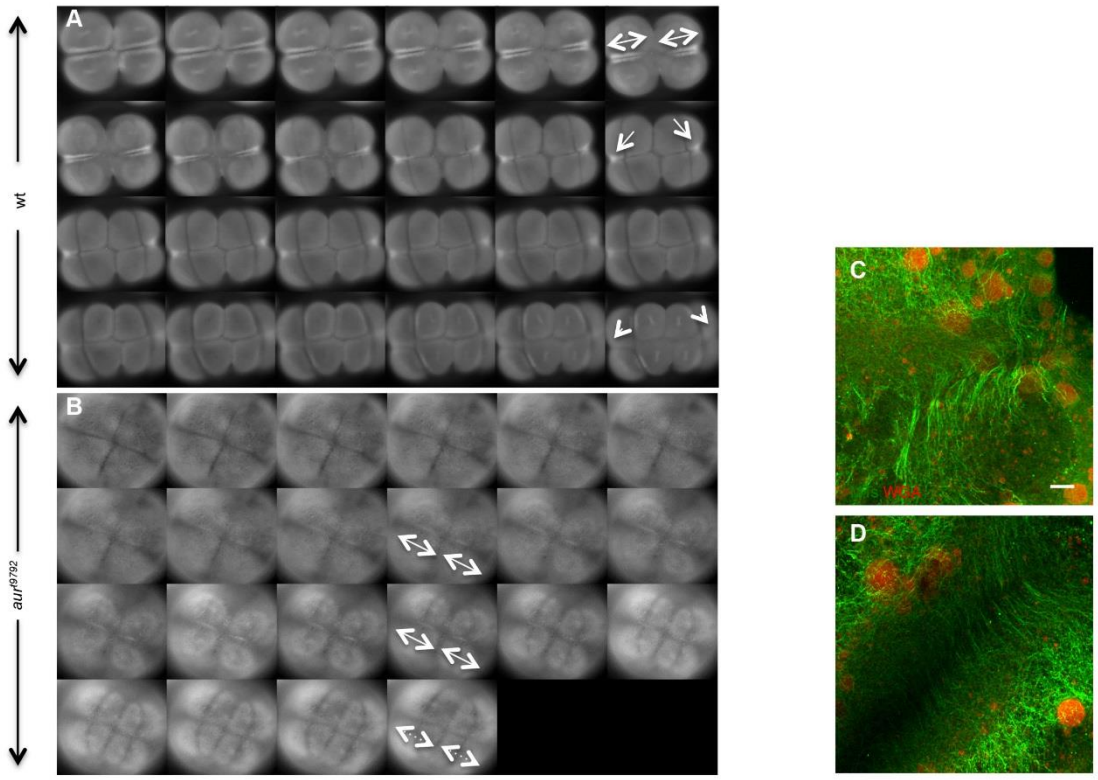

Supplementary Figure 4: Lack of FMA reorganization in *aura* embryos. Live imaging of microtubules in embryos using the EMTB transgene in wild-type and *aura* mutant line. (A) In wild-type, the FMA forms along the furrow (double arrows), compacts distally (arrows) and disappears (arrowheads). (B) In *aura* mutant embryos, the FMA also appears along the furrow (double arrows), but does not experience a distal shift and remains in an apparently stabilized condition until it eventually becomes undetectable (dotted line arrows). Images were taken in one minute intervals from 60 mpf to 85 mpf. (C,D) Microtubule reorganization defect occurs independently of the number of ectopic CGs in *aura* mutants. In *aura* mutants, the FMA appears stabilized in all (100%) embryos, regardless of the number of ectopic CGs at the furrow: (C) furrow with ≥ 5 GCs (6/16 examined furrows); (D) furrow with ≤ 4 CGs (10/16 examined furrows). Furrows shown are examples of the 1st furrow of a single embryo at 75 mpf, when the FMA has normally become either distally enriched or disassembled (Urven et al, 2006). Similar results are obtained with the 2nd furrow (not shown) Scale bar: C,D, 10 µm

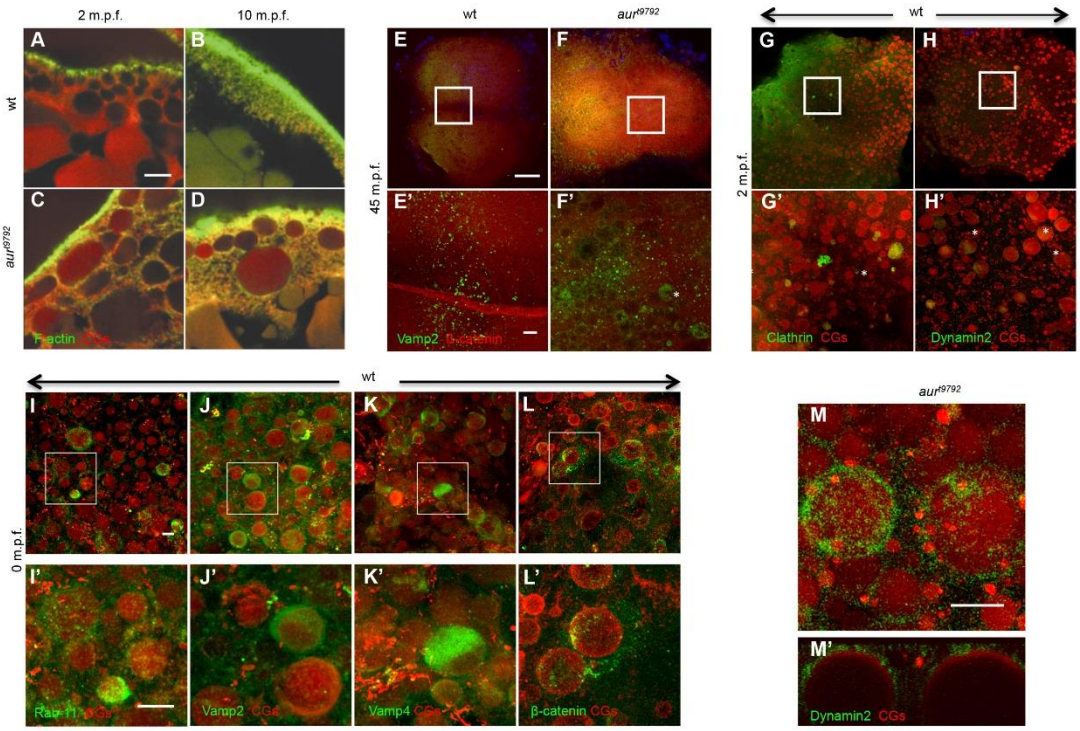

Supplementary Figure 5: Membrane dynamics of wild-type and *aura* mutant embryos. (A-D) Side view of wild-type (A,B) and *aura* mutant (C,D) embryos at 2 mpf and 10 mpf, labeled to detect F-actin and CGs, showing that mutants exhibits a similar localization of CGs at the cortex during egg activation (A,C) and retains a fraction of CGs (B,D). (E-F) In wild-type at 45 mpf, β-catenin localizes to the furrow but Vamp2 does not yet localize to this structure (4/4 embryos) (E, E') In *aura* mutants, Vamp2 appears localize to ectopic CGs (8/9 embryos) (F,F'). Vamp2 also localizes to small cortical particles in both wild-type and mutant embryos (E', F'). (G-L) Localization of Clathrin (G, G'), Dynamin2 (H,H'), Rab11 (I,I'), Vamp2 (J,J'), Vamp4 (K,K'), and ß-catenin (L,L') to a subset of CGs in wild-type at 2 mpf (G-H) or 0 mpf (I-L). (M, M') Dynamin2 surrounding CGs in *aura* mutant embryos as seen by a face-on view (M) and a reconstructed orthogonal view (M'). Scale bars: A-D (bar in A): 10 µm; E-H (bar in E): 100 µm; E'-H'(bar in E'): 10 µm; I-M' (bar in I,I',M): 10 µm.

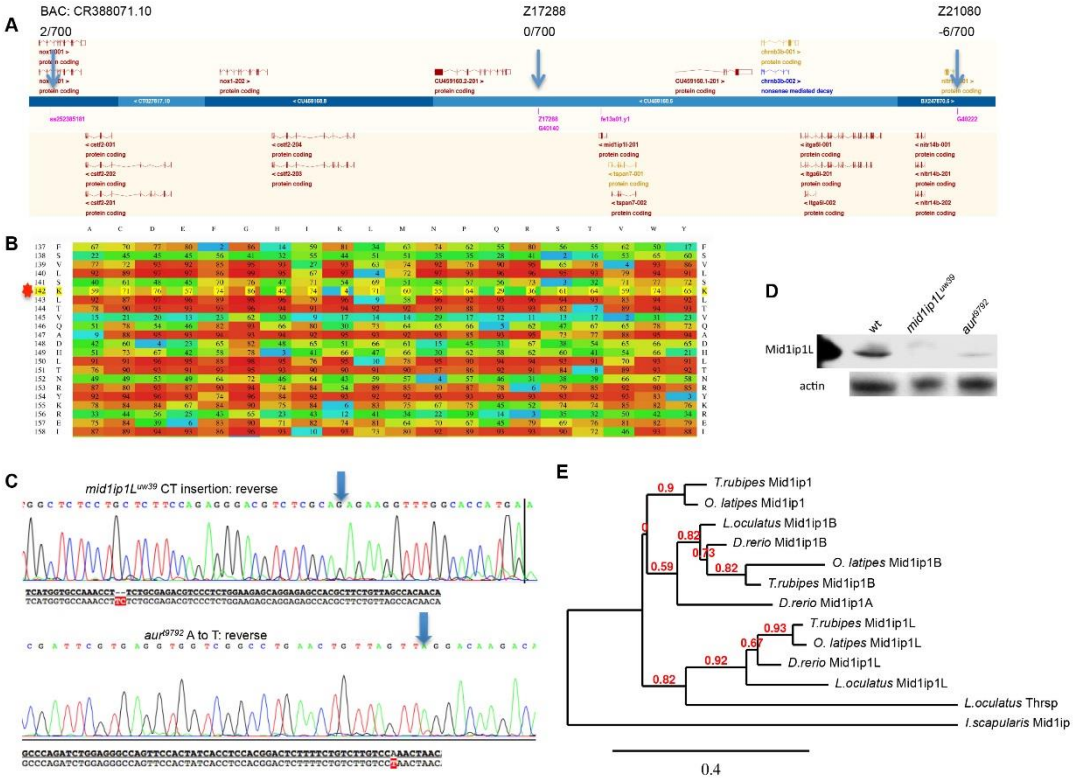

Supplementary Figure 6: (A) Location of *mid1ip1L* on chromosome 14. Ensembl depiction of *mid1ip1L* location with SSLP markers used for cloning and number of recombinants. See Methods for details. (B) SuSPect protein phenotypic prediction analysis of the *aur*^{t9792} allele. SuSPect missense analysis software predicts a severe phenotype will result with an amino acid change in residues following that in which the *aur*^{t9792} mutation generates a stop codon (red asterisk), suggesting that the truncation would result in a loss-of-function allele. Values represent probability of the amino acid change causing a deleterious mutation, where 50 is defined as the cutoff between neutral and disease-causing variant, color-coded with red showing the strongest predicted deleterious effect on function. (C) Confirmation of the genotype of *aur*^{t9792}*/mid1ip1L*^{uw39} heterozygous females used in the genetic complementation test. Representative Sanger sequencing chromatograms of DNA derived from *aur*^{t9792}*/mid1ip1L*^{uw39} females. The analysis confirms the presence of the two *mid1ip1L* alleles in the same female: the CRISPR-generated *mid1ip1L*^{uw39} two-base pair insertion sequence and the A-to-T transversion corresponding to the original *aur*^{t9792} mutation. Wild-type and mutant sequence for the sense strand (complementary to that of the trace, which corresponds to the antisense strand) are shown below the trace, comparing wild-type (top) and mutant (bottom) sequences and with inserted bases and mutation highlighted in red. (D) Western blot

of whole protein lysates from wild-type, *mid1ip1L*^{uw39}, and *aur*^{t9792} at 45 mpf using Mid1ip1L and actin antibodies. E) Phylogenetic tree for various Mid1ip1 protein sequences focusing on fish lineages: *L. oculatis* (spotted gar), *T. rubipes* (Torafugu or Japanese Puffer fish), *O. latipes* (medaka fish), and *D. rerio*, with *I. scapularis* (deer tick) as an outgroup. Numbers in red indicate branch support values, number in black indicates branch scale bar. The gene phylogenetic tree is consistent with an early split between A/B and L forms, and a subsequent split between A and B forms.

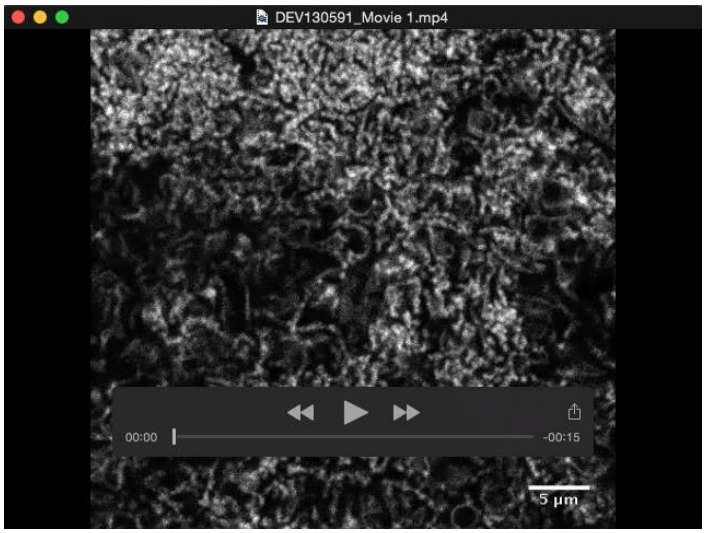

Supplementary Movie 1. Imaging of F-actin in live wild-type embryos using the LifeAct transgene. Images from 17 through 22 mpf, with frames taken every 2 seconds. Magnification as in Fig. 8, panels A'E'. F-actin exhibits dramatic patterns of reorganization, which temporarily coalesce into band-like structures.

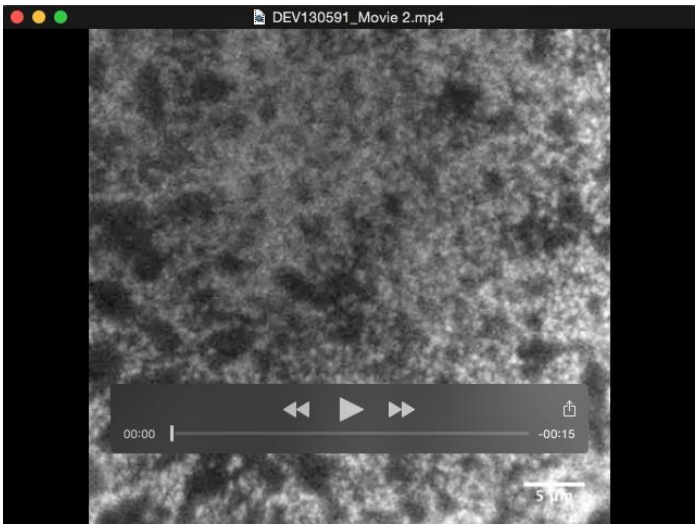

Supplementary Movie 2. Imaging of F-actin in live *aura* mutant embryos using the LifeAct transgene. Images from 17 through 22 mpf, with frames taken every 2 seconds. Magnification as in Fig. 8, panels F'-J'. *aura* mutants show an absence of wave-like dynamic reorganization observed in wild-type. Instead, F-actin appears relatively stationary as it remains as aggregates. The observed gradual bulk cortical movement is likely caused by slight tilting of the embryo during imaging.

Table S1. Primers

Primer Name	5'-3'	Use
mid1ip1L N'term F	GGATCTTTCTTCTCTGCTGAGTCT	genotyping
mid1ip1L N'term R	GTCCAACAATTCACGAACAGTCTA	genotyping
mid1ip1L C'term F	GCGCTAATATAGACTGTTCGTGA	genotyping
mid1ip1L N'term R	CATTACAGCACAATATAAAAATTGAAG	genotyping
in situ F	CAAGCACTCGCTGCTCAATG	Antisense *in situ*
in situ (T7)+*mid1ip1L* R	(gaaattaatacgactcactatagg) TCGCAATAAGCTTCCCCCGC	Antisense *in situ*
in situ (T7)+*mid1ip1L* F	(gaaattaatacgactcactatagg) ATGATGCAGCTCAGCAACGA	Sense *in situ*, mRNA
in situ R	CCCGCCGATTTCTCTCTTGT	Sense *in situ*, mRNA
mid1ip1a F	AGCCAGAAGAACGCTCTCTACAC	RTPCR
mid1ip1a R	AATGCCAATCTCCTGCTTGTAT	RTPCR
mid1ip1b F	AAATCTGCGACTCCTACAACCAA	RTPCR
mid1ip1b R	CCACATCCACCAATACCAATTTC	RTPCR
mid1ip1L F	CAAGCACTCGCTGCTCAATG	RTPCR
mid1ip1L R	CCCGCCGATTTCTCTCTTGT	RTPCR
ß-actin1 F	GCCCATCTATGAGGGTTACG	RTPCR
ß-actin1 R	AGGAAGGAAGGCTGGAAGAG	RTPCR
mid1ip1L sgRNA	(gatttaatacgactcactata)CCTTCTGCGAGACG TCCCTC (gtttagagctagaa)	CRISPR generation
Universal Primer	Aaaagcaccgactcggtgccacttttcaagttgataa cggactagccttattttaacttgctatttctagctctaaaac	CRISPR generation
PCR primer for *aura*^{t9792} F	TTTTCCGACGCAAATGTGTAATG	sequencing
PCR primer for *mid1ip1L*^{uw39} F	CATGGTGCCAAACCTTCTCT	sequencing
R Primer both alleles	GGGGAATCTCGAGACCTT	sequencing
NestF *aura*^{t9792}	GGGGAATCTCGAGACCTT	sequencing
NestR *mid1ip1L*^{uw39}	GCCATCTCCCGCTTCAAAAG	sequencing